# OXYGEN DOPED GRAPHITIC CARBON NITRIDE PHOTOCATALYSTS: PHYSICAL-CHEMICAL AND PHOTOCATALYTIC PROPERTIES

**Bakhromova I.A[1], Kattaev N.T[1], Akbarov Kh.I[1], Sidrasulieva G.B[2].**

*[1]National university of Uzbekistan, PhD student, Uzbekistan*
*[1]National university of Uzbekistan, associate professor, Uzbekistan*
*[1]National university of Uzbekistan, professor, Uzbekistan*
*[2]Karakalpak State university, PhD teacher, Karakalpakstan*
***E-mail:*** *irodabaxromova1@gmail.com*

**Abstract:** ***Background.*** Using the photocatalytic activity of graphitic carbon nitrides in the visible light field, it is possible to determine the reaction order of the destruction of organic dyes.
**Patient and Method:** The concentration of intermediate and final substances obtained by photocatalytic destruction of rhodamine B dye was measured by spectrophotometric method. **Results:** Oxygen-doped graphitic carbon nitride was synthesized by the thermal polycondensation method. Their infrared spectrum, XRD analysis, surface structure morphology, thermal analysis, and photocatalytic properties were studied. The bandgap was 2.64 eV in O-g-$C_2N_3$. The destruction of rhodamine B in the presence of oxygen-doped graphitic carbon nitride (O-g-$C_2N_3$) was studied under the influence of ultraviolet, visible and sunlight. The photocatalytic destruction of rhodamine B followed a first-order reaction. **Conclusion:** Oxygen doped (O-g-$C_3N_4$ O-g-$C_2N_3$) photocatalysts were synthesized by thermal polycondensation method from dicyandiamide. The obtained new materials (O-g-$C_3N_4$, O-g-$C_2N_3$) were used for the photocatalytic decomposition of rhodamine B under the influence of visible, ultraviolet (UV) and sunlight. The new materials showed high photocatalytic activity under the influence of sunlight and degraded organic dyes up to 97%.

***Keywords:*** oxygen doped graphitic carbon nitrides, bandgap, rhodamine B, photocatalytic destruction.

## INTRODUCTION

The photocatalytic degradation method is based on the degradation of organic pollutants in the presence of UV-Vis light and a photocatalyst material. Graphitic carbon nitride (g-$C_3N_4$) is the most efficient photocatalyst material used for the degradation of organic pollutants from water and wastewaters g-$C_3N_4$ has good chemical stability and physical properties, high degradation capacities of organic pollutants, is easy to use, and respects the environmental system. g-$C_3N_4$ is a semiconductor polymer with a graphite-layered structure composed of nitrogen and carbon atoms [1]. The negative conduction band potential of this promising semiconductor material provides a strong driving force for the water reduction reaction [2]. However, g-$C_3N_4$ prepared by traditional methods exhibits low conversion efficiency of solar energy owing to the rapid recombination of photoinduced electron-hole pairs and limited light absorption capacity, thus restricting its practical application. As a result, it is critical to optimize g-$C_3N_4$ for improved photocatalytic performance

by, among other things, constructing heterojunctions, morphological modulation, chemical group modification, coupling with other semiconductors, and doping with heteroatoms [3-4]. The most common precursors used to prepare g-$C_3N_4$ are melamine, dicyandiamide, cyanimide, urea, thiourea, and ammonium thiocyanate. Among different types of carbon nitrides, such as α-$C_3N_4$, β-$C_3N4$, cubic $C_3N_4$, pseudo cubic $C_3N_4$, with bandgaps of around 5.49 eV, 4.85 eV, 4.30 eV, and 4.13 eV, respectively, g-$C_3N_4$ is the most stable phase under ambient conditions [5]. In order to enhance the performance and modulate the properties of g-$C_3N_4$, researchers have proposed different methods, such as doping and making heterojunction with other materials. Examples of these materials are metal oxides, metal sulfides, noble metals, and carbonaceous nanomaterials [6-8]. The surface morphology, particle size, electronic and optical properties, as well as a number of other physical-chemical properties of g-$C_3N_4$ change when nonmetallic elements are doped into it. Pure g-$C_3N_4$ absorbs light up to 420 nm, while the doping of a non-metallic element increases the absorption of visible light and reduces the recombination of photoinduced electrons and holes.

The most common ways to introduce elemental oxygen into g-$C_3N_4$ are oxidation methods, such as oxidation of g-$C_3N_4$ with acids [9], thermal oxidation [10], oxidation of hydrogen peroxide $H_2O_2$ [11], hydrothermal treatment [12], pretreatment of synthetic precursors followed by thermal oxidation [13], and solvothermal methods [14].

The efforts of various research groups to improve the photocatalytic activity of g-$C_3N_4$ in processes of $CO_2$ reduction, $H_2$-evolution, and organic contaminants degradation by its non-metal doping were successful. Their results confirmed that g-$C_3N_4$ is a universal, environmentally friendly, low-priced, and stable material for creating new photocatalysts with targeted properties. Graphitic carbon nitrides can also be used in the degradation of organic dyes.

Rhodamine B (RhB), as a typical organic dye, is very stable under visible light irradiation and is a carcinogen. Many technologies, such as adsorption, photodegradation, chemical oxidation, biological technology, and so on, have been developed to remove organic dyes from wastewater. Semiconductor photocatalysis has the advantages of low energy consumption, high efficiency, and excellent chemical stability, making it a green and low-cost technology for organic pollutant degradation [15-16].

**Aim of the study:** Determination of the reaction order of the photocatalytic destruction of rhodamine B dye in the presence of oxygen-doped graphitic carbon nitrides by graphical method.

**PATIENT AND METHOD**

The phase composition of the obtained samples was studied by X-ray diffractometry using a multifunctional powder diffractometer (XRD) from X-Pert Pro Panalytical using Cu Kα radiation (k = 1.54056 Å). The measurements were taken at Bragg angles ranging from 10-80°, with a scanning step of 0.01° and a shooting time of 1 s. The architectural information of the samples was analyzed using the Fourier transform infrared (FT-IR) spectra of the samples embedded in KBr pellets (Nicolet iS50, Thermo Scientific, USA). The optical absorption spectra of the materials were measured in diffuse reflectance mode using an EMC-30PC-UV/VIS Spectrophotometer (Germany). Scanning electron microscope analysis and energy dispersion X-ray spectroscopy (SEM-EDX, Jeol JSM-IT200LA, Japan) The bandgap of photocatalysts calculated by diffuse reflectance spectra was recorded using an Eye-One Pro (i1 Pro) mini-spectrophotometer—a monitor calibrator (X-Rite, Switzerland). Thermal analysis was carried out by the methods of differential thermogravimetry (DTG) and differential scanning calorimetry (DSC) using the synchronous thermal analysis device "Simultaneus DTA-TG apparatus", Shimadzu, Japan. Thermograms were taken in the following conditions: corundum crucible, air atmosphere,

temperature range 30-900 ºC, sample heating rate 10 ºC/min, sample weight 10 mg. Reverse-phase nano-LC-MS/MS was performed using the Agilent 1200 nano-flow LC system connected to the CHIP-Q-TOF Agilent Technologies 6520B series mass spectrometer. The sample was fractionated using an Agilent Technologies 1200 series chromatograph with a Zorbax SB C18. 5 µm, 75 mm x 43 mm chip. A: 0.1% formic acid solution + 5% acetonitrile; B: acetonitrile + 0.1% formic acid + 10% deionized water. The application was carried out on an Agilent Technologies 1260 Cap Pump device at a flow rate of 4 µl/min. The elution was carried out on an Agilent Technologies.

**RESULTS**

The required amount of dicyandiamide was placed in a special autoclave made of a stainless steel vessel and synthesized by the thermal polycondensation method at 550 °C for the synthesis of O-g-$C_3N_4$. As a result of the thermal decomposition of dicyandiamide in a ceramic crucible in the presence of air oxygen at 550 C for 3 hours, ammonia was released and oxygen-doped graphitic carbon (O-g-$C_3N_4$) with a porous structure was formed.

$CN_x$ nanofibers were prepared by the calcination of polypyrrole (PPy) nanowires at 800 °C in a special autoclave made of stainless steel. PPy nanowires were prepared as follows: polypyrrole (PPy) was chemically synthesized in water (50 ml) by mixing a solution of pyrrole (Py) of 0.043 M with an oxidizing solution of $FeCl_3$ (0.1 M). The synthesis was allowed to proceed at 20 °C. The pyrrole solution was kept in the bath before adding $FeCl_3$. Molar ratio of $FeCl_3$/Py = 2.3:1 Following the reaction, the precipitate was filtrated and thoroughly washed with deionized water before being dried overnight at 70 °C. PPy nanowires were calcinated at 800 °C in a special autoclave made of stainless steel and a furnace for 2 h, and $CN_x$ nanofibers were obtained. O-g-$C_2N_3$ was prepared as follows: a certain amount of $CN_x$ was placed in a glass, and 30 mL of a hot ethanol solution containing 10 g of dicyandiamide was poured into the glass. The mixture was then ultrasonically treated for 30 minutes and dried at 70 °C for 12 hours. The obtained powder was placed in a stainless steel special autoclave and calcined at 550 °C for 3 hours in an air muffle furnace, yielding O-g-$C_2N_3$ and a $CN_x$ amount of 0.4 g.

The process of synthesizing a new photocatalyst was carried out in several stages. The process of formation of an oxygen-doped photocatalyst obtained by thermal polycondensation reaction in the presence of air is shown in the following diagram:

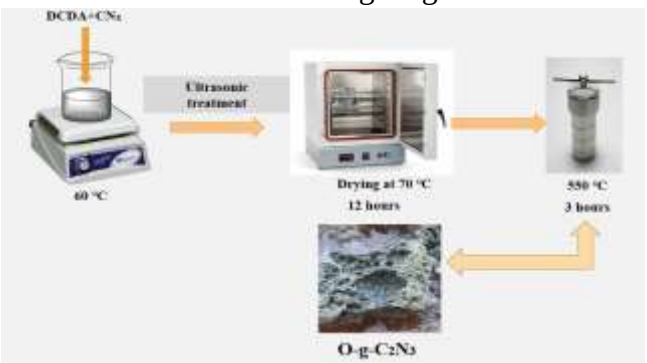


**Figure 1. Synthesis of O-g-$C_2N_3$ photocatalyst**

An olive-colored porous substance was formed as a result of the synthesis.

**DISCUSSION**

The phase composition of O-g-$C_2N_3$ was identified by XRD (Figure 2a).

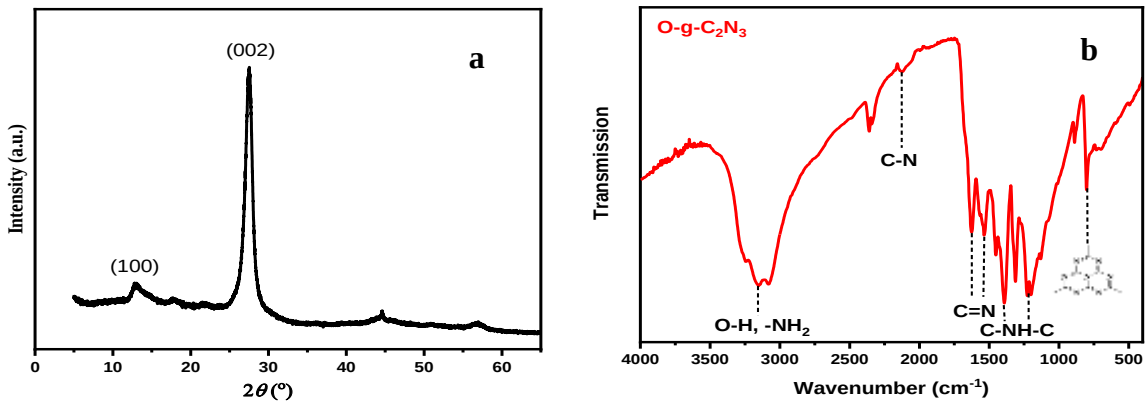


**Figure 2. XRD patterns(a) and Fourier-IR spectrum (b) of O-g-$C_2N_3$.**

XRD patterns (a) of O-g-$C_2N_3$ samples derived from polypyrrole and dicyandiamide. Respectively, where it can be seen that there exist two distinct diffraction peaks for O-g-$C_2N_3$. These two diffraction peaks occur at 13.28° and 27.38°. For the two peaks, the stronger one is generated by the stacking of the conjugated aromatic ring, indexed as the (002) crystal plane for graphite-like materials [17]; while, the weaker one is attributed to the in-plane ordering of tri-s-triazine units, assigned as the (100) crystal plane [18].

Absorption at 802 $cm^{-1}$ in the IR spectra of O-g-$C_2N_3$ (Fig. 2(b)) is typical for tri-s-triazine, vibrations at 1200-1600 $cm^{-1}$ are due to C-N(-C)-C and C-NH-C bridges, and absorption at 3078 $cm^{-1}$ corresponds to -OH and -$NH_2$ groups. Due to the moisture in the sample, a vibration characteristic of the -OH group was observed in the IR spectrum. The absorption at 3078 $cm^{-1}$ may also correspond to a typical melem group. The vibrations at 494.2, 699.1 $cm^{-1}$ as well as 1227.3 and 1537.8 $cm^{-1}$ correspond to the heptazine ring. In addition, absorption at 1622.2 $cm^{-1}$ is associated with the C=N group [20].

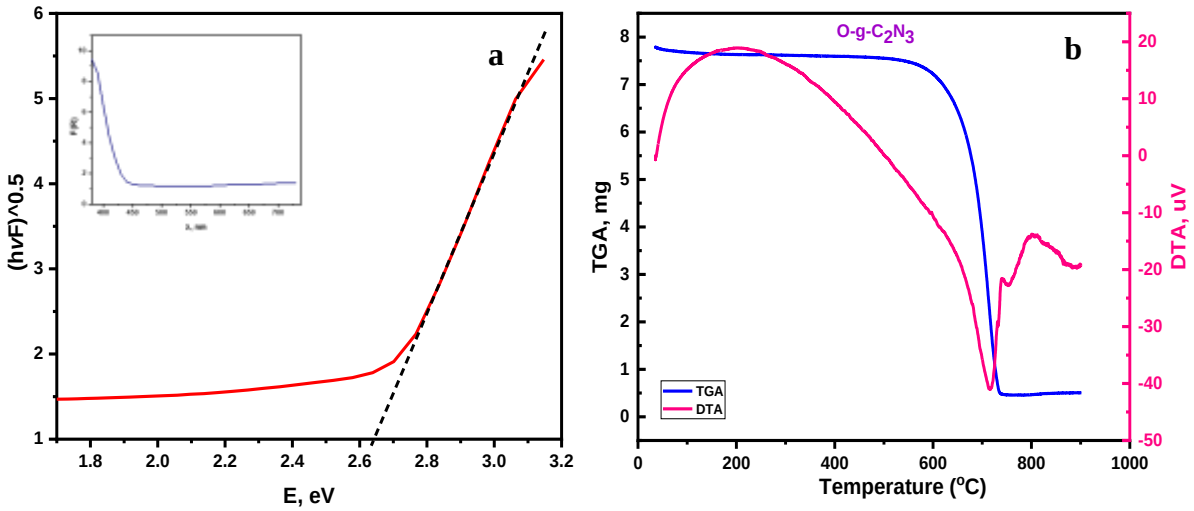


**Figure 3. Light diffusion reflection spectrum and Tauc curve of O-g-$C_2N_3$ photocatalyst (a), TGA and DTA curves (b) of sample O-g-$C_2N_3$.**

The electronic structure of the photocatalyst O-g-$C_2N_3$, was studied using light diffusion reflection spectroscopy (DRS). To determine the bandgap of O-g-$C_2N_3$, photocatalyst, the following Kubelka-Munk equation was used (Figure 3a):

$$F(R)h\nu = A\left(h\nu - E_g\right)^2$$

The bandgap of the O-g-$C_2N_3$, photocatalyst was determined graphically using the Tauc curve.

The $h\nu$ - $(F(R)h\nu)^{1/2}$ dependence was used to calculate the O-g-$C_2N_3$ bandgap, was found to be 2.64 eV. This indicates that the synthesized O-g-$C_2N_3$ has semiconducting properties and has a high potential to exhibit photocatalytic activity in the visible light field.

Figure 3(b) shows the O-g-$C_2N_3$ derivatogram. When O-g-$C_2N_3$ is heated to 400 ℃, melen is formed. The main reason for the loss of mass in this temperature range is due to the release of ammonia. When heating to 600℃ is continued, melon is formed due to the polymerization of melem. O-g-$C_2N_3$ is very thermally stable at temperatures below 600 ℃, at temperatures above 630 ℃ it decomposes to lower molecular compounds (such as $CO_2$, $NH_3$). As can be seen from the TG curve of O-g-$C_2N_3$, a mass loss of -3.004% was observed in the range of 35.49-495.02 ℃, and a mass loss of -90.96% was observed in the range of 495.97-742.49 ℃. It can be seen that in the temperature range of 35-495 ℃, energy absorption is related to dehydration and thermal deformation, and in the temperature range of 495-742 ℃, thermal/thermal-oxidative degradation occurs. With thermal deformation, the loss of the multi-layer structure or the heptazine chains of graphitic carbon nitride is observed.

As can be seen from the above results, the composition of the samples is very thermally stable in a wide temperature range. This shows that the obtained materials can be used in a wide temperature range.

The photocatalytic activity of the obtained materials was studied in laboratory conditions. To quantify the photocatalytic process destruction of rhodamine B by graphitic materials (O-g-$C_3N_4$, O-g-$C_2N_3$), a spectroscopic method of analysis in the region 190-1000 nm was used.

The main absorption peak (RhB 554 nm) of photocatalytic degradation of solutions was studied using a UV-visible spectrometer. Photocatalytic degradation efficiency was calculated by using the below equation:

$$Degradation\ efficiency = \frac{C}{C_0} \times 100\ \%$$

Where, $C_0$- is the initial concentration; C-concentration at time (mg/L).

The photocatalytic activity of the synthesized oxygen-doped photocatalysts against rhodamine B was studied. The results of the study of the photocatalytic destruction of rhodamine B under the influence of UV, visible light, and sunlight in the presence of a photocatalyst containing O-g-$C_2N_3$ are presented in Fig. 4.

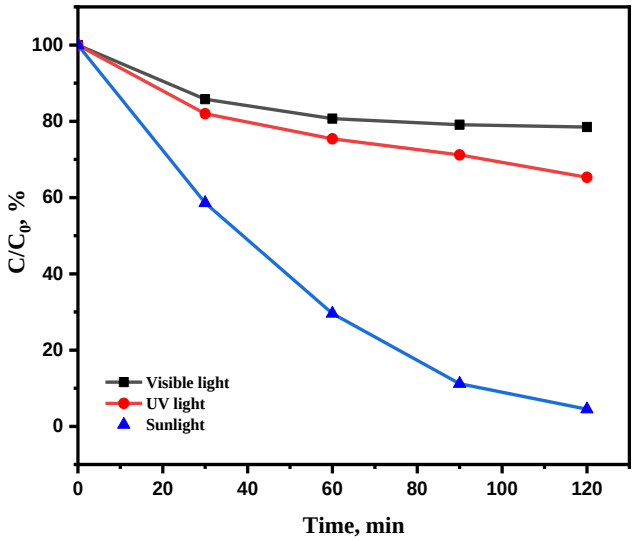


**Figure 4. Destruction curves of Rhodamine B (10 mg/L) under the influence of UV, visible and sunlight in the presence of photocatalyst (O-g-$C_2N_3$).**

The destruction of rhodamine B (Fig. 4) under the influence of UV and visible light in the presence of the O-g-$C_2N_3$ photocatalyst was 25–30%, and under the influence of sunlight, this indicator was 95–97%.

The best indicator was obtained when the destruction of rhodamine B was studied under the influence of UV, visible light, and sunlight. Therefore, destruction processes in other concentrations were carried out under the influence of sunlight. Sunlight contains up to 5% UV (10-380 nm), 45-50% visible (380-730 nm) and 50-55% infrared (730 nm-10 μm).

Graphitic carbon nitrides use light rays to form $e^-/h^+$ pairs on their surface. The e-/h+ pair then creates conditions for the destruction process and active states of oxygen, HO, and $O_2$, and these pairs cause pollutant decomposition. The kinetics of the zero (1), first (2), and second (3) order reactions of the destruction of rhodamine B dye with different concentrations under the influence of sunlight in the presence of O-g-$C_3N_4$, O-g-$C_2N_3$ photocatalysts were studied (Fig.5-6) [19].

$$C_0-C=k_0t \quad (1)$$

$$\ln(C_0/C) =k_1t \quad (2)$$

$$1/C=k_2t+1/C_0 \quad (3)$$

Here:

C and $C_0$ are the initial and dye concentration at time t;

$k_0$, $k_1$, $k_2$ are rate constants of zero, first and second order reactions, respectively.

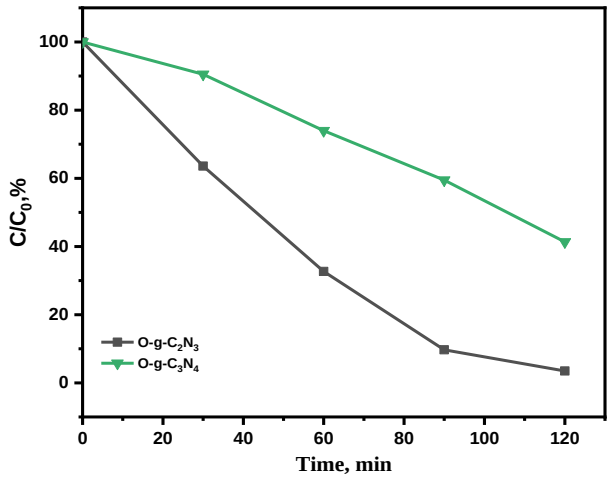


**Figure 5. Destruction curves of rhodamine B (10 mg/L) under the influence of sunlight in the presence of photocatalysts (O-g-$C_3N_4$, O-g-$C_2N_3$).**

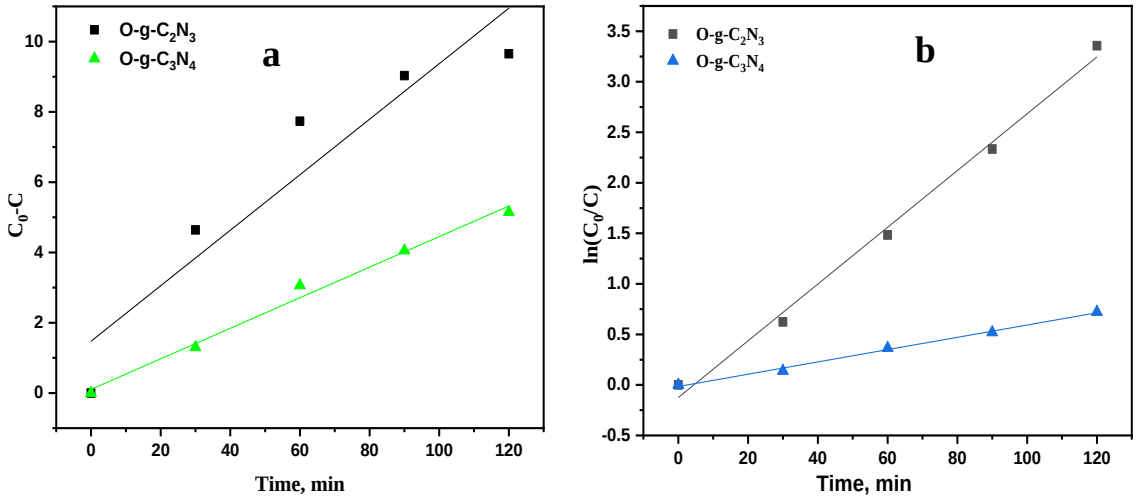

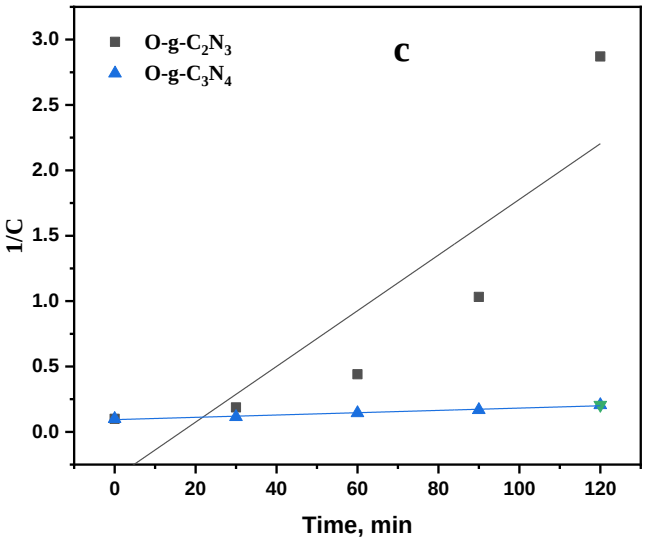


**Figure 6. Zero (a), first (b), second (c) order kinetic models of rhodamine B (10 mg/L) dye degradation with O-g-$C_3N_4$, O-g-$C_2N_3$ photocatalysts.**

Using the above formulas, the kinetic models of the zeroth, first, and second order reactions of rhodamine B dye destruction were found graphically. The rate constants and $R^2$ values were determined by calculations (Table 1). The graphs are given above (Fig. 6).

**Table 1.**

**Kinetic constants calculated from the destruction of rhodamine B in the presence of photocatalysts.**

| № | Photocatalyst | Zero order | | First order | | Second order | |
|---|---|---|---|---|---|---|---|
| | | $k_0$ | $R^2$ | $k_1$ | $R^2$ | $k_2$ | $R^2$ |
| 1 | O-g-$C_3N_4$ | 0.0494 | 0.9863 | 0.0060 | 0.9941 | $8.83 \cdot 10^{-4}$ | 0.97.41 |
| 2 | O-g-$C_2N_3$ | 0.0780 | 0.8520 | 0.0286 | 0.9911 | 0.0213 | 0.7016 |

The kinetics of the destruction of RhB (10 mg/L) under the influence of sunlight in the presence of photocatalysts was studied by various kinetic models (Table 1). From the values in the table above, it became clear that the destruction of organic dye with the participation of photocatalysts corresponds to the kinetic model of the first-order reaction. From this, it can be concluded that only the amount of paint changes during the destruction process.

Degradation intermediates of RhB were recognized by positive ion mode mass spectra for products after 120 min. Degradation of a rhodamine B solution containing 10 mg/L. The initial solution, the solution after degradation for 120 min were analyzed by HPLC-MS, and the components of the photodegradation products were analyzed. The photocatalytic degradation mechanism of rhodamine B by O-g-$C_2N_3$ catalyst was also studied.

For the initial solution, a mass peak at m/z 443 was observed, which is attributed to the RhB molecule of a chloride ion. Peaks at m/z 415 and 387 are assigned to the deethylated intermediates of RhB. The peak at m/z 318 originates from the intermediates of m/z 387 after losing a fragment of 74 mass units, {$(C_2H_5)_2NH$}. The decarboxylation product of m/z 274 was also observed. Peak at m/z 141 is attributed to C9 compounds with an oxygen atom, respectively. For the mass spectra

of products after 120 minutes, the signals of macromolecular intermediates were very weak. These results suggest that RhB was broken down into small molecules in 120 minutes, which were eventually decomposed into $CO_2$ and $H_2O$. A large number of experiments and mass spectrometry data proved that RhB photodegradation was a process that included gradual deethylation and breakage of the double bond in the benzene ring. The degradation mechanism is shown in Fig. 7.

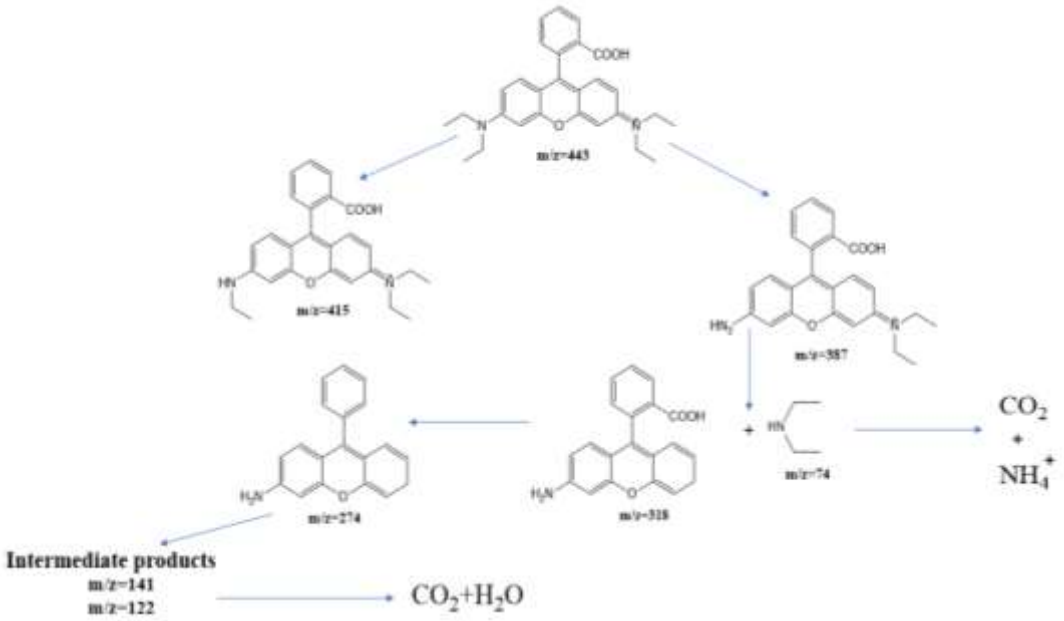


**Figure 7. Proposed degradation mechanism of Rhodamine B**

Under the influence of sunlight, electrons and holes in the O-g-$C_2N_3$ photocatalyst move to an excited state. Photoinduced charge carriers interact with $OH^-$ and $O_2$ to form $^*OH$ and $O_2^{*-}$. The breakdown of Rhodamine B and the photocatalytic reactions that can occur are given below:

1. O-g-$C_2N_3$+hν ⟶ $e^-+h^+$
2. $O_2+e^-$ ⟶ $O_2^{*-}$
3. $H_2O$ ⟶ $OH^-+H^+$
4. $OH^-+h^+$ ⟶ $^*OH$
5. $O_2^{*-}+H^+$ ⟶ $HO_2^*$
6. $HO_2^*+e^-$ ⟶ $HO_2^-$
7. $HO_2^-+H^+$ ⟶ $H_2O_2$
8. $H_2O_2+e^-$ ⟶ $^*OH+OH^-$
9. Rhodamine B+$^*OH$ ⟶ degradation product

Rhodamine B + $h^+$ ⟶ oxidation product

Rhodamine B + $e^-$ ⟶ reduction product

As can be seen from the above results, the synthesized photocatalysts undergo photocatalytic destruction of organic pollutants under the influence of visible light. Therefore, these photocatalysts can easily be used for environmental purposes.

**CONCLUSION**

Oxygen doped O-g-$C_2N_3$ photocatalyst was synthesized by thermal polycondensation method from dicyandiamide and polypyrrole. The diffractograms of newly synthesized photocatalysts revealed that their structure consists of non-uniform crystals, explained, apparently, with recrystallization initial grains during synthesis. The study of the electronic structure by spectroscopy diffuse reflection, it is proved that the obtained materials have improved semiconductor properties, bandgap of O-g-$C_2N_3$ is 2.64 eV.

The obtained new materials (O-g-$C_3N_4$, O-g-$C_2N_3$) were used for the photocatalytic decomposition of rhodamine B under the influence of visible, UV and sunlight. The new materials showed high photocatalytic activity under the influence of sunlight and degraded organic dyes up to 97%.

To study the mechanism of the photodegradation process, chromato-mass analyzes were taken, and through these results, approximate mechanisms of the degradation process for rhodamine B was proposed.

## REFERENCES

1. X. Wang, K. Maeda, A. Thomas, K. Takanabe, G. Xin, J. Carlsson, K. Domen, M. Antonietti, A metal-free polymeric photocatalyst for hydrogen production from water under visible light, *Nat. Mater.*, 2009, **8**, 76-80.

2. Q. Xu, B. Zhu, C. Jiang, B. Cheng, J. Yu, Constructing 2D/2D $Fe_2O_3$/g-$C_3N_4$ direct Z-scheme photocatalysts with enhanced $H_2$ generation performance, *Sol. RRL*, 2018, **2**, 1800006.

3. A. Kumar, M. Khan, J. He, I. M. C. Lo, Visible-light-driven magnetically recyclable terephthalic acid functionalized g-$C_3N_4$/$TiO_2$ heterojunction nanophotocatalyst for enhanced degradation of PPCPs, *Appl. Catal. B*, 2020, **270**,118898.

4. R. Zhang, L. Bi, D. Wang, Y. Lin, X. Zou, T. Xie, Z. Li, Investigation on various photo-generated carrier transfer processes of $SnS_2$/g-$C_3N_4$ heterojunction photocatalysts for hydrogen evolution, *J. Colloid Interf. Sci.*, 2020, **578**, 431-440.

5. Ong, W.-J.; Tan, L.-L.; Ng, Y.H.; Yong, S.-T.; Chai, S.-P. Graphitic Carbon Nitride (g-$C_3N_4$)-Based Photocatalysts for Artificial Photosynthesis and Environmental Remediation: Are We a Step Closer to Achieving Sustainability? *Chem. Rev.* **2016**, *116*, 7159–7329.

6. Jiang, H.; Li, Y.; Wang, D.; Hong, X.; Liang, B. Recent Advances in Heteroatom Doped Graphitic Carbon Nitride (g-$C_3N_4$) and g-$C_3N_4$/Metal Oxide Composite Photocatalysts. *Curr. Org. Chem.* **2020**, *24*, 673–693.

7. Wang, L.; Wang, C.; Hu, X.; Xue, H.; Pang, H. Metal/Graphitic Carbon Nitride Composites: Synthesis, Structures, and Applications. *Chem. Asian J.* **2016**, *11*, 3305–3328.

8. Gotipamul, P.P.; Vattikondala, G.; Rajan, K.D.; Khanna, S.; Rathinam, M.; Chidambaram, S. Impact of Piezoelectric Effect on the Heterogeneous Visible Photocatalysis of g-$C_3N_4$/Ag/ZnO Tricomponent. *Chemosphere* **2022**, *287*, 132298.

9. C. Zhou, C. Lai, C. Zhang, G. Zeng, D. Huang, M. Cheng, L. Hu, W. Xiong, M. Chen, J. Wang, Y. Yang and L. Jiang, Appl. Catal., B, 2018, 238, 6-18.

10. X. Li, J. Yu, S. Wageh, A. A. Al-Ghamdi and J. Xie, Small, 2016, 12, 6640-6696.

11. Chen, W.; Jiang, D.; Zhu, M.Y.; Shi, T.Y.; Li, H.N.; Wang, K. An effective strategy for fabricating highly dispersed nanoparticles on O-C3N4 with enhanced electrocatalytic activity and stability. J. Alloy. Compd. 2018, 741, 1203–1211.

12. Yousefi, M.; Villar-Rodil, S.; Paredes, J.I.; Moshfegh, A.Z. Oxidized graphitic carbon nitride nanosheets as an effective adsorbent for organic dyes and tetracycline for water remediation. J. Alloy. Compd. 2019, 809, 11.

13. Zhu, W.R.; Hao, N.; Lu, J.W.; Dai, Z.; Qian, J.; Yang, X.D.; Wang, K. Highly active metal-free peroxidase mimics based on oxygen-doped carbon nitride by promoting electron transfer capacity. Chem. Commun. 2020, 56, 1409–1412.

14. Chubenko, E.B.; Baglov, A.V.; Leonenya, M.S.; Yablonskii, G.P.; Borisenko, V.E. Structure of Photoluminescence Spectra of Oxygen-Doped Graphitic Carbon Nitride. J. Appl. Spectrosc. 2020, 87, 9–14.

15. Denisov, N.M.; Chubenko, E.B.; Bondarenko, V.P.; Borisenko, V.E. Synthesis of Oxygen-Doped Graphitic Carbon Nitride from Thiourea. Tech. Phys. Lett. 2019, 45, 108–110.

16. Gao, Y.W.; Zhu, Y.; Lyu, L.; Zeng, Q.Y.; Xing, X.C.; Hu, C. Electronic Structure Modulation of Graphitic Carbon Nitride by Oxygen Doping for Enhanced Catalytic Degradation of Organic Pollutants through Peroxymonosulfate Activation. Environ. Sci. Technol. 2018, 52, 14371–14380.

17. Liu Q, Zhang JY. Graphene supported Co-g-$C_3N_4$ as a novel metal-macrocyclic electrocatalyst for the oxygen reduction reaction in fuel cells. Langmuir. 2013; 29: 3821–3828. doi: 10.1021/la400003h PMID: 23425296

18. Zhang JS, Chen XF, Takanabe K, Maeda K, Domen K, Epping J, et al. Synthesis of a carbon nitride structure for visible-light catalysis by copolymerization. Angew Chem Int Ed. 2010; 49: 441–444.

19. Nasrin Khorshidi, Saied Abedini Khorrami, Mohammad Ebrahim Olya, Fereshteh Mo., 2015, Photodegradation of Basic Dyes using Nanocomposite (Silver Zinc Oxide- Copper Oxide) and Kinetic Studies, OJCHEG 2016, Vol. 32, No. (2): Pg. 1205-1214.

20. I.A. Bakhromova, N. T. Kattaev, Kh.I. Akbarov, O.N. Ruzimuradov. Synthesis and photocatalytic properties of new graphitic carbon nitride // Journal of Chemistry of Uzbekistan. - 2022. - No. 4. -Pg. 9-14.